

## Aircraft vertical profiles of trace gas and aerosol pollution over the mid-Atlantic United States: Statistics and meteorological cluster analysis

B. F. Taubman,<sup>1</sup> J. C. Hains,<sup>2</sup> A. M. Thompson,<sup>1</sup> L. T. Marufu,<sup>3</sup> B. G. Doddridge,<sup>3</sup> J. W. Stehr,<sup>3</sup> C. A. Piety,<sup>3</sup> and R. R. Dickerson<sup>3</sup>

Received 19 May 2005; revised 28 July 2005; accepted 18 August 2005; published 29 March 2006.

[1] From 1997 to 2003, airborne measurements of O<sub>3</sub>, CO, SO<sub>2</sub>, and aerosol properties were made during summertime air pollution episodes over the mid-Atlantic United States (34.7–44.6°N, 68.4–81.6°W) as part of the Regional Atmospheric Measurement, Modeling, and Prediction Program (RAMMPP). Little diurnal variation was identified in the CO, SO<sub>2</sub>, and Ångström exponent profiles, although the Ångström exponent profiles decreased with altitude. Boundary layer O<sub>3</sub> was greater in the afternoon, while lower free tropospheric O<sub>3</sub> was invariant at ~55 ppbv. The single scattering albedo increased from morning to afternoon ( $0.93 \pm 0.01 - 0.94 \pm 0.01$ ); however, both profiles decreased with altitude. A cluster analysis of back trajectories in conjunction with the vertical profile data was used to identify source regions and characteristic transport patterns during summertime pollution episodes. When the greatest trajectory density lay over the northern Ohio River Valley, the result was large O<sub>3</sub> values, large SO<sub>2</sub>/CO ratios, highly scattering particles, and large aerosol optical depths. Maximum trajectory density over the southern Ohio River Valley resulted in little pollution. The greatest afternoon O<sub>3</sub> values occurred during periods of stagnation. North-northwesterly and northerly flow brought the least pollution overall. The contribution of regional transport to afternoon boundary layer O<sub>3</sub> was quantified. When the greatest cluster trajectory density lay over the Ohio River Valley (~59% of the profiles), transport accounted for 69–82% of the afternoon boundary layer O<sub>3</sub>. Under stagnant conditions (~27% of the profiles), transport only accounted for 58% of the afternoon boundary layer O<sub>3</sub>. The results from this study provide a description of regional chemical and transport processes that will be valuable to investigators from the Baltimore, New York, and Pittsburgh EPA Supersites.

**Citation:** Taubman, B. F., J. C. Hains, A. M. Thompson, L. T. Marufu, B. G. Doddridge, J. W. Stehr, C. A. Piety, and R. R. Dickerson (2006), Aircraft vertical profiles of trace gas and aerosol pollution over the mid-Atlantic United States: Statistics and meteorological cluster analysis, *J. Geophys. Res.*, *111*, D10S07, doi:10.1029/2005JD006196.

### 1. Introduction

[2] In 1992, in response to mounting air pollution problems over the mid-Atlantic United States, the Regional Atmospheric Measurement Modeling and Prediction Program (RAMMPP, <http://www.atmos.umd.edu/~RAMMPP/>) was formed. RAMMPP comprises four elements, measurements (ground-based and airborne), chemical transport modeling (Models-3/CMAQ), mesoscale modeling (MM5), and air quality forecasting, aimed at conducting holistic, long-term air quality studies in the region and

analyzing transboundary pollution transport processes. The airborne measurements have been conducted by the University of Maryland since 1992 with an instrumented light aircraft outfitted for atmospheric research. The aim of the aircraft analyses thus far has been to answer specific questions regarding lower atmospheric CO [Dickerson *et al.*, 1995; Doddridge *et al.*, 1998], pollutant transport and boundary layer dynamics during individual, mid-Atlantic haze and O<sub>3</sub> episodes [Ryan *et al.*, 1998; Taubman *et al.*, 2004a], and the air quality and radiative impacts of smoke in the mid-Atlantic from Canadian forest fires [Taubman *et al.*, 2004b]. Additionally, a fortuitous experiment demonstrated the regional air quality benefits of the 2003 North American blackout [Marufu *et al.*, 2004]. The objective of this study is to answer some of the overarching questions not yet addressed by these case studies. To that end, a cluster analysis of back trajectories was used together with the comprehensive RAMMPP aircraft data set to answer the following questions: (1) Is there a statistical link between characteristic regional transport patterns into the mid-Atlan-

<sup>1</sup>Department of Meteorology, Pennsylvania State University, University Park, Pennsylvania, USA.

<sup>2</sup>Department of Chemistry and Biochemistry, University of Maryland, College Park, Maryland, USA.

<sup>3</sup>Department of Meteorology, University of Maryland, College Park, Maryland, USA.

tic United States during summertime haze and O<sub>3</sub> episodes and specific pollution loadings? (2) Can the local O<sub>3</sub> contributions be differentiated from regionally imported O<sub>3</sub>; if so, are the regional contributions quantifiable?

[3] *Moody and Galloway* [1988] appear to be the first to have used clustering techniques similar to those employed in this paper. Since then, other studies [e.g., *Dorling et al.*, 1992a; *Dorling et al.*, 1992b; *Lee et al.*, 1994; *Moy et al.*, 1994; *Dorling and Davies*, 1995; *Moody et al.*, 1995; *Harris and Oltmans*, 1997; *Brankov et al.*, 1998; *Moody et al.*, 1998; *Cape et al.*, 2000; *Eneroth et al.*, 2003; *Berto et al.*, 2004; *Jorba et al.*, 2004; *Russell et al.*, 2004] have also conducted this type of analysis. Specifically, the impacts of emissions and meteorology on pollutant concentrations at receptor sites have been analyzed via the clustering of back trajectories to determine source regions and the synoptic regimes that support the regional transport of different atmospheric constituents. The main distinctions among the studies lie in the different methods used to calculate the trajectories and the different techniques used to cluster the trajectories.

[4] The major limitation of the published studies arises from the fact that all of the receptor sites were surface based. This restricts the amount of information available on regional transport and the influences of lower atmospheric dynamics on the pollution measured at the surface. Certain studies [e.g., *Eneroth et al.*, 2003; *Jorba et al.*, 2004] clustered trajectories at multiple altitudes to better describe the general circulation patterns in the troposphere, but the measurements were still fixed at the surface. The study presented herein improves upon the previous studies by using similar statistical techniques to analyze several years of data collected from an aircraft, which can be considered a mobile receptor site. Also, for the first time, a climatology of both trace gas and aerosol properties based on the clustering technique is presented.

[5] Aircraft provide a horizontally and vertically mobile sampling platform. The horizontal mobility allows for deployment to specific areas of interest, while the vertical mobility provides insight into boundary layer dynamics, and allows for measurements representative of a larger area. The ability to deploy to specific locations enables the investigation of multiday haze and O<sub>3</sub> episodes, the influences of regionally transported pollution on urban and rural areas as well as the impacts large metropolitan areas have on mid-Atlantic air quality. The vertical profile information presents a more complete picture of the composition and dynamics of the lower atmosphere, which facilitates an investigation of the factors influencing the transport and chemical transformations of air pollutants and their precursors. Namely, the nocturnal emissions from elevated sources and transport of pollution in the residual layer are calculated from vertical profiles taken before the stable, nocturnal boundary layer has eroded and the pollution mixed down to the surface. The identification of transported pollution allows for a more accurate assessment of the effects of mixed layer development on surface pollution as well as local emissions and photochemical production.

[6] The mobile nature of the sampling platform necessitated a novel approach to clustering the data. There were limited individual locations over which enough flights were performed to provide statistical meaning

using the typical analysis. Furthermore, narrowly focusing on a few locations would fail to take advantage of the regional coverage offered by the data set. Ozone events have long been identified as regional in nature with variability expected on scales of hundreds of km [*Logan*, 1985], so the use of multiple spatially heterogeneous receptor locations is justified. Still, the standard distance calculations used in the cluster algorithm had to be modified to account for the spatial variability. Additionally, a statistical analysis of vertical profiles is inherently different from analyses of single measurements at surface-based receptor sites. A detailed description of the methods is presented below (section 2). The statistical techniques employed allowed for a quantification of the impacts of source regions and transport patterns on mid-Atlantic air quality (section 3). The measurements from this study overlap in time with those from the mid-Atlantic EPA Supersites in Baltimore, New York, and Pittsburgh. Because of the regional nature of this study, the results presented herein will be useful to the investigators from those sites, aiding in measurement inter-comparisons, model validation, and understanding the processes that control regional pollutant transport to and between the individual sites. The analyses should also be useful for air quality forecasting and modeling of pollution episodes as well as pollution control strategies.

## 2. Observations

### 2.1. Sampling Platform and Instrumentation

[7] Extensive descriptions of the sampling platform, a twin engine Piper Aztec research aircraft, and instruments have been published [*Taubman et al.*, 2004b], so only a brief summary is provided. The specifications are summarized in Table 1.

[8] Geographic position was measured with a Garmin GPS-90. Static pressure was measured inside the unpressurized cabin of the aircraft using a Rosemount Model 2008 pressure transducer. Temperature and relative humidity were measured with a Rustrak RR2-252 probe using a thermistor and capacitive thin film, respectively.

[9] Ozone data were acquired with a commercial, UV photometric based O<sub>3</sub> analyzer (TEI Model 49). For observations of CO, a high-performance, modified [*Dickerson and Delany*, 1988] commercial, nondispersive infrared gas filter correlation analyzer (TEI Model 48) was used. A modified, commercial, pulsed fluorescence detector (TEI Model 43C) was used for measurements of ambient SO<sub>2</sub> [*Luke*, 1997].

[10] Particle light absorption was measured with a Particle/Soot Absorption Photometer (PSAP, Radiance Research). The detection limit (95% confidence level) for S:N = 1 is  $0.9 \times 10^{-6} \text{ m}^{-1}$  [*Anderson et al.*, 1999; *Bond et al.*, 1999] when 1-min measurement averages are used. Particle light scattering was quantified using an integrating nephelometer (TSI Model 3563) that measures the particle scattering at 450, 550, and 700 nm after correcting for light scattered by the walls of the measurement chamber, the sample gas, and any electronic noise [*Anderson et al.*, 1996]. Corrections were made to the measurements to account for forward scattering angular truncation and non-Lambertian distribution of illumination intensity within the

**Table 1.** Values Measured, Instruments Used, Measurement Units, and the Periods Over Which Measurements Were Made

Species	Instrument	Units	Measurement Period
Position	Garmin GPS-90	latitude, longitude	1997–2003
Static pressure	Rosemount Model 2008 pressure transducer	mb	1997–2003
Temperature	Rustrak RR2-252 thermistor	°C	1997–2003
Relative humidity	Rustrak RR2-252 capacitive thin film	%	1997–2003
O <sub>3</sub>	TEI Model 49	ppbv	1997–2003
CO	TEI Model 48	ppbv	1999–2003
SO <sub>2</sub>	TEI Model 43C	ppbv	2000–2003
Particle scattering	TSI Model 3563	m <sup>-1</sup>	2001–2003
Particle absorption	Particle/Soot Absorption Photometer	m <sup>-1</sup>	2001–2003

nephelometer [Anderson and Ogren, 1998]. Measurements of light scattering were made after the sample airflow was dried from ambient conditions to a relative humidity of <20%. For the corrections made to account for hygroscopic growth, see Taubman *et al.* [2004a].

## 2.2. Measurements

[11] All flights analyzed for this study were conducted in the summertime (June, July, and August) and were specifically designed to characterize regional, episodic pollution events. The observations reported herein therefore represent polluted periods, not background values. The flight locations used in this analysis, while not listed individually, represent a fairly complete cross section of the mid-Atlantic, from 34.7 to 44.6°N and 68.4 to 81.6°W.

[12] The flights consisted of transects between small, regional airports over which vertical survey spirals between the surface and roughly 3 km above ground level were conducted at  $\sim 100 \text{ m min}^{-1}$ . The spirals were performed with the smallest possible radius and each one took approximately 30 min to complete. It is assumed that horizontal and general atmospheric variability over the brief time interval are minimal, so that the spirals represent a near-instantaneous vertical column of the lowest 3 km of the atmosphere.

[13] From 1997 through 2003, there were 550 summertime flights, which included 255 morning spirals (before noon local standard time (LST), average time 0930 LST) and 295 afternoon spirals (after noon LST, average time 1330 LST). The median profiles for the morning and afternoon vertical profiles of O<sub>3</sub>, CO<sub>2</sub>, SO<sub>2</sub>, the single scattering albedo at 550 nm ( $\omega_{0.550}$ ), and Angström exponent ( $\alpha$ ) from the 450/700 (nm) ratio of total scattering are shown in Figure 1. The profiles were generated by calculating the median value at each altitude layer from all of the measured profiles.

[14] The morning O<sub>3</sub> profile (Figure 1a) shows relatively small values ( $\sim 45$ – $55$  ppbv) within the nocturnal boundary layer (roughly the lowest 500 m), with considerably more O<sub>3</sub> in the residual layer above. This disparity is typically the result of surface deposition and titration with freshly emitted NO within the nocturnal boundary layer combined with nighttime regional transport from upwind sources within the residual layer. Solar heating induces a more thoroughly mixed afternoon O<sub>3</sub> profile with photochemical production adding to that which was transported overnight. Above approximately 2 km, the morning and afternoon values are nearly identical ( $\sim 55$  ppbv), indicating a summertime episodic background value that may be transported long range.

[15] The morning and afternoon CO profiles (Figure 1b) are nearly identical below  $\sim 1$  km, with large values near the surface that fall off with altitude. The shape of the vertical profiles is similar to those presented by Dickerson *et al.* [1995], although the absolute values presented herein are slightly greater than in the previous study. Above 1 km, the afternoon values are slightly larger than the morning, indicating convective outflow from the boundary layer, the preamble to long-range transport.

[16] The SO<sub>2</sub> profiles (Figure 1c) show little difference between the morning and afternoon. The afternoon profile shows somewhat smaller values near the surface, likely the result of oxidation to SO<sub>4</sub><sup>2-</sup>. There is also evidence of vertical mixing in the afternoon; however, both profiles show greater values near the surface that decrease with altitude. Sulfur dioxide is a fairly short lived species (typically less than a day in summertime when clouds are present, considering reactions with OH and H<sub>2</sub>O<sub>2</sub> as well as dry deposition) with sources generally elevated slightly above the surface. The decline with altitude could be a result of oxidation by H<sub>2</sub>O<sub>2</sub> in fair weather cumulus (common under summertime high-pressure systems and often encountered during these flights) as SO<sub>2</sub> mixes vertically [e.g., Kleinman and Daum, 1991].

[17] The  $\omega_{0.550}$  afternoon boundary layer average is greater than the morning profile ( $0.94 \pm 0.01$  vs.  $0.93 \pm 0.01$ ) (Figure 1d), presumably the result of SO<sub>2</sub> oxidation to SO<sub>4</sub><sup>2-</sup>, the primary scattering component in fine particles over the eastern United States. Both profiles decrease considerably above 2 km. The absorption was relatively invariant with altitude, so the decline in  $\omega_{0.550}$  with altitude is driven by a decrease in scattering values. These observations are consistent with those of Novakov *et al.* [1997], who reported an increase in the relative amounts of carbonaceous to SO<sub>4</sub><sup>2-</sup> species with altitude over the eastern United States coastline. No diurnal pattern in  $\alpha$  was observed (Figure 1e); however a slight decrease with altitude is apparent in both the morning and afternoon profiles. The presence of larger particles aloft may be due to particle growth through preferential aging in the lower free troposphere as articulated by Taubman *et al.* [2004a].

## 2.3. Trajectory Calculations

[18] Back trajectories are a standard tool for determining the source regions and transport patterns of air parcels observed at receptor sites. While they may not represent the exact transport path of an air parcel, back trajectories are good representations of the general three-dimensional wind flow and are useful in identifying particular synoptic sit-

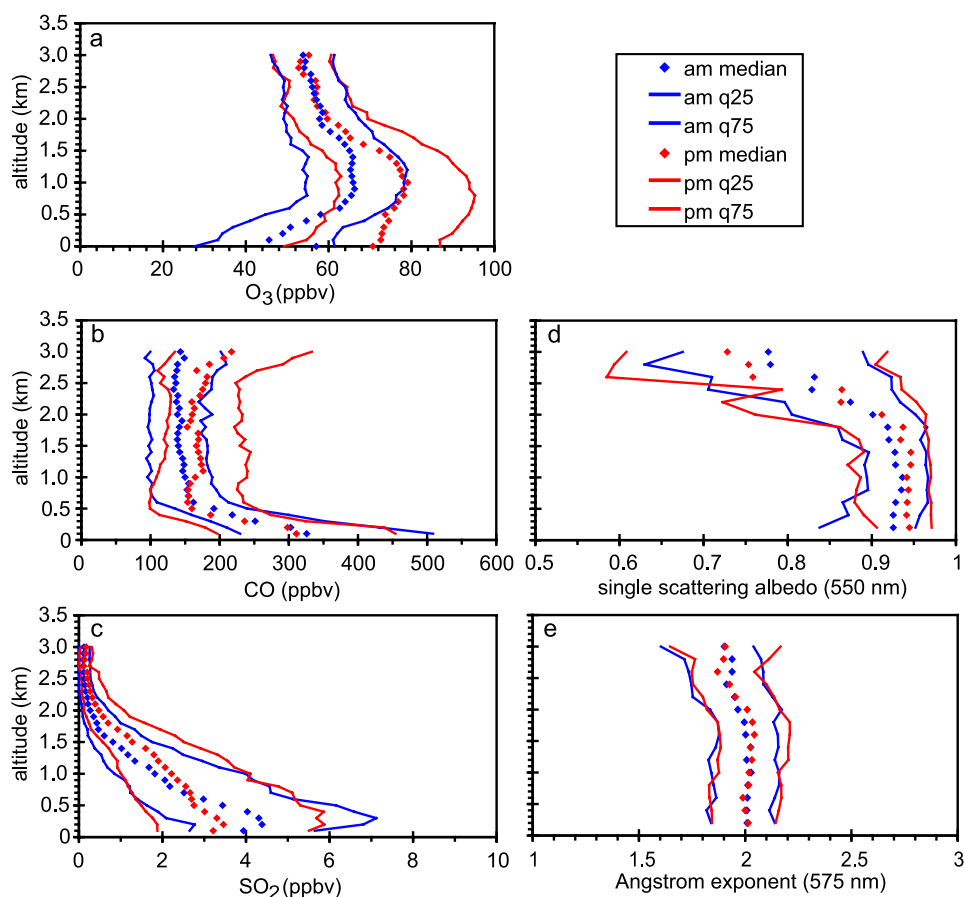


**Figure 1.** Median values calculated every 100 m from all morning (blue, before 1200 LST) and afternoon (red, after 1200 LST) profiles for (a) O<sub>3</sub> (255 morning profiles, 295 afternoon profiles), (b) CO (118 morning profiles, 134 afternoon profiles), (c) SO<sub>2</sub> (176 morning profiles, 206 afternoon profiles), (d) single scattering albedo (550 nm) (122 morning profiles, 138 afternoon profiles), and (e) Angstrom exponent (575 nm) (142 morning profiles, 153 afternoon profiles). The solid lines indicate the 1st and 3rd quartiles for the morning (blue) and afternoon (red) profiles.

uations. The accuracy and errors associated with the different estimations of air parcel trajectories have been quantified [Stohl *et al.*, 1995; Stunder, 1996; Stohl, 1998]. Individual trajectories may be subject to errors; however, clustering multiple trajectories together minimizes errors and uncertainties.

[19] Forty-eight hour, three-dimensional kinematic back trajectories were calculated from the time and location of every aircraft spiral using the NOAA Air Resources Laboratory (ARL) HYbrid Single-Particle Lagrangian Integrated Trajectory (HY-SPLIT) model (version 4) [Draxler and Rolph [2003], <http://www.arl.noaa.gov/ready/hysplit4.html>] and 80 km Eta Data Assimilation System (EDAS) 3-hourly archive data. Kinematic back trajectories were used because, owing to improvements to the accuracy of the vertical wind component, they have been shown to be more accurate than other methods (e.g., isentropic and isobaric) [Stohl *et al.*, 1995; Stohl and Seibert, 1998; Stohl, 1998; Jorba *et al.*, 2004]. Two-day back trajectories were long enough to capture regional transport patterns and short enough to keep trajectory errors, which accumulate with simulation time, to a minimum. The air parcel latitudes, longitudes, and pres-

ures were recorded at 1 h intervals. Trajectories were calculated starting at 1, 2, and 3 km (above ground level).

## 2.4. Cluster Analysis

[20] For each trajectory starting altitude (1, 2, and 3 km), a separate cluster analysis was performed. These starting altitudes describe the vertical range over which the aircraft vertical survey spirals were performed. By clustering the trajectories at each of the three altitudes, any variations in the atmospheric circulation patterns in the lower atmosphere and the impacts on regional transport could be identified. The results of the cluster analysis for the three altitudes were similar. The 2 km trajectory cluster results were used for the remainder of the analysis because this altitude is near the middle of the aircraft spirals and most representative of the entire spiral.

[21] The trajectories trace a three-dimensional path through time to the receptor site. To determine the similarity among individual trajectories, the total variability between each trajectory pair must be quantified. The variability may be calculated as a scalar distance between trajectories. At each time step, the position of the air parcel is defined by its latitude, longitude, and pressure. These data were converted

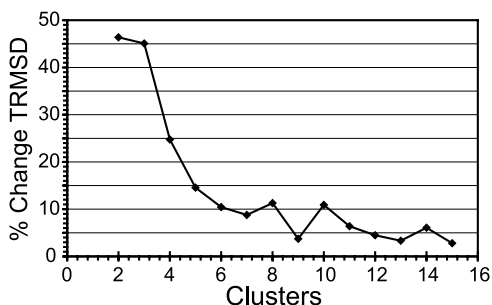


**Figure 2.** Percent change in the total root mean square deviation (TRMSD) calculated by summing the root mean square deviation of each cluster versus the number of total clusters.

to Cartesian coordinates by treating the Earth as a sphere and calculating their position in three-dimensional space.

[22] The vertical and horizontal distances traveled by air parcels along trajectory paths may have commensurate impacts on pollutant values at a receptor site. However, the vertical spatial distances covered are typically less than the horizontal ones in an equivalent time step. Thus, without normalizing the three-dimensional coordinates, the vertical component may not have an equal weighting in the distance calculation of the cluster analysis. A normalization procedure was therefore applied to account for the disproportionality. The mean value for each coordinate at every time step was calculated. The differences between the individual coordinates and their mean values were quantified at every time step. These differences were then divided by an amount equivalent to one standard deviation from the mean value. In this way, the coordinates were all converted to a normalized distance from the mean value of that particular coordinate, thereby giving equal weighting to all three coordinates in the cluster analysis.

[23] The Euclidean distance,  $D$ , between each trajectory pair was calculated according to the equation:

$$D_{ij} = \sqrt{\sum_{k=1}^n (x_{ik} - x_{jk})^2 + (y_{ik} - y_{jk})^2 + (z_{ik} - z_{jk})^2} \quad (1)$$

In the above equation,  $D$  is the three-dimensional distance between the two trajectories under comparison, represented here by the subscripts  $i$  and  $j$ . The variables  $x$ ,  $y$ , and  $z$  represent the normalized distances from the means of the Cartesian coordinates. The number of time steps used in the analysis is given by  $k$  (48 for hourly time steps over 2 days). However, the first six time steps back from the receptor site were given zero weighting to account for the spatial heterogeneity of the aircraft spiral locations. To further discount the spatial variability of the receptor locations and place the emphasis on the source regions, the trajectory time steps were weighted linearly back in time [e.g., Lee *et al.*, 1994], increasing the weighting for each hour after the initial six zero-weighted time steps.

[24] After the distances between individual trajectories were calculated, the trajectories were clustered using an agglomerative, hierarchical clustering algorithm. The algorithm used an average linkage function, where the average

distances between all pairs of objects in clusters  $i$  and  $j$  are calculated, to determine the distances between the trajectories making up the clusters. Average linkage minimizes the within-cluster variance while maximizing between-cluster variance and has been identified as an effective method for categorizing different synoptic situations [Kalkstein *et al.*, 1987]. Newly formed clusters were linked to other trajectories to create successively larger clusters until all of the trajectories were connected by a hierarchical dendrogram. The algorithm has no inherent mechanism for identifying an appropriate terminus for this iterative process. Barring manual intervention, all objects are eventually grouped into one cluster. So, the final number of clusters was specified arbitrarily from 1 to 15 clusters.

[25] The appropriate number of clusters was determined by first calculating an “average” trajectory, or trajectory center, for each cluster. The root mean square deviation (RMSD) of each trajectory within a cluster from the cluster center was quantified. The RMSDs were then summed to give the total root mean square deviation (TRMSD). The percent change in the TRMSD was plotted against the total number of clusters [e.g., Cape *et al.*, 2000; Brankov *et al.*, 1998] (Figure 2). Large changes were interpreted as the merging of significantly different trajectories into the same cluster. Accordingly, the appropriate number of clusters would be found just prior to the large percent change in TRMSD. While this technique lends objectivity to the analysis, a subjective interpretation of the optimal number of clusters based on the meteorology and pollutant profiles as well as what value constitutes a large enough percent change in TRMSD is still required. When eight clusters were merged into fewer clusters the change in TRMSD remained consistently high ( $\sim 10\%$ ) and grew larger upon further agglomeration. After reviewing the meteorology and pollutant profiles associated with each cluster, eight was determined to be the appropriate number of clusters.

## 3. Results and Discussion

### 3.1. Cluster Solution

[26] The eight cluster solution is shown in Figure 3 with trajectory “spaghetti” plots of each cluster. The relative density of air parcel locations in each cluster, however, is better described by trajectory density plots, given in Figure 4. A linear interpolation method was used to generate values between the original trajectory latitude and longitude points. The locations of the largest (top 0.3%) annual  $\text{NO}_x$  and  $\text{SO}_2$  emitters in the eastern United States (EPA AirData Facility Emissions Report—Criteria Air Pollutants 1999, <http://www.epa.gov/air/data/>) are overlaid on the trajectory density maps. The trajectory densities represent the relative amount of time the air parcels from every trajectory in a cluster spent over the total areas defined by the trajectories before reaching the receptor location. This is a technique based on the “residence time analysis” [Ashbaugh, 1983] and it will be shown below that it is an effective means of determining downwind pollutant loadings.

[27] Most flights were conducted during multiday pollution episodes. The characteristic synoptic patterns associated with each cluster were analyzed using NCEP reanalysis data [Kalnay *et al.*, 1996] from the NOAA-CIRES Climate Diagnostics Center to make composite mean plots of the

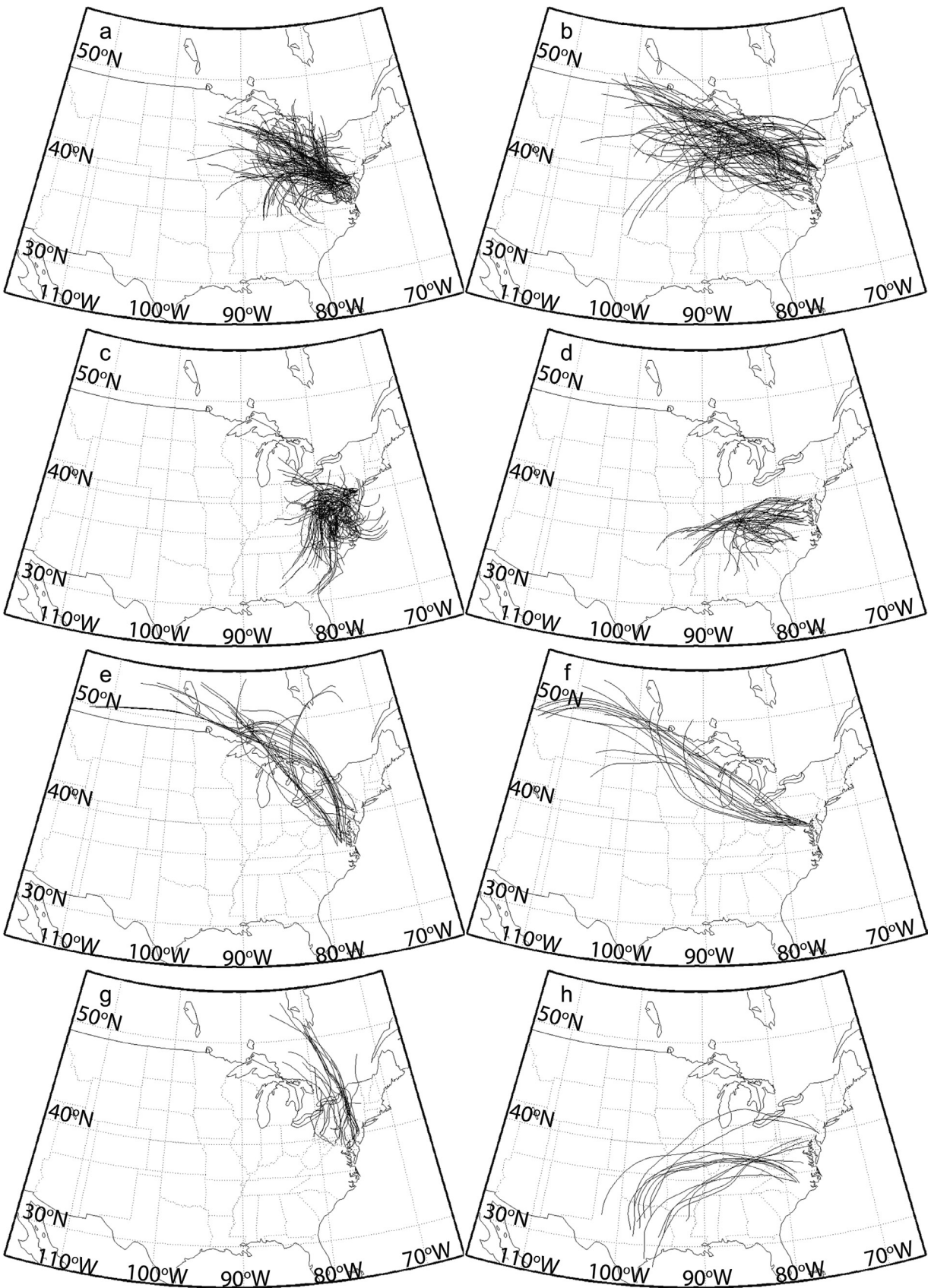


**Figure 3.** Maps showing the 2 km, 48 h HY-SPLIT back trajectories that make up (a) cluster 1, (b) cluster 2, (c) cluster 3, (d) cluster 4, (e) cluster 5, (f) cluster 6, (g) cluster 7, and (h) cluster 8.

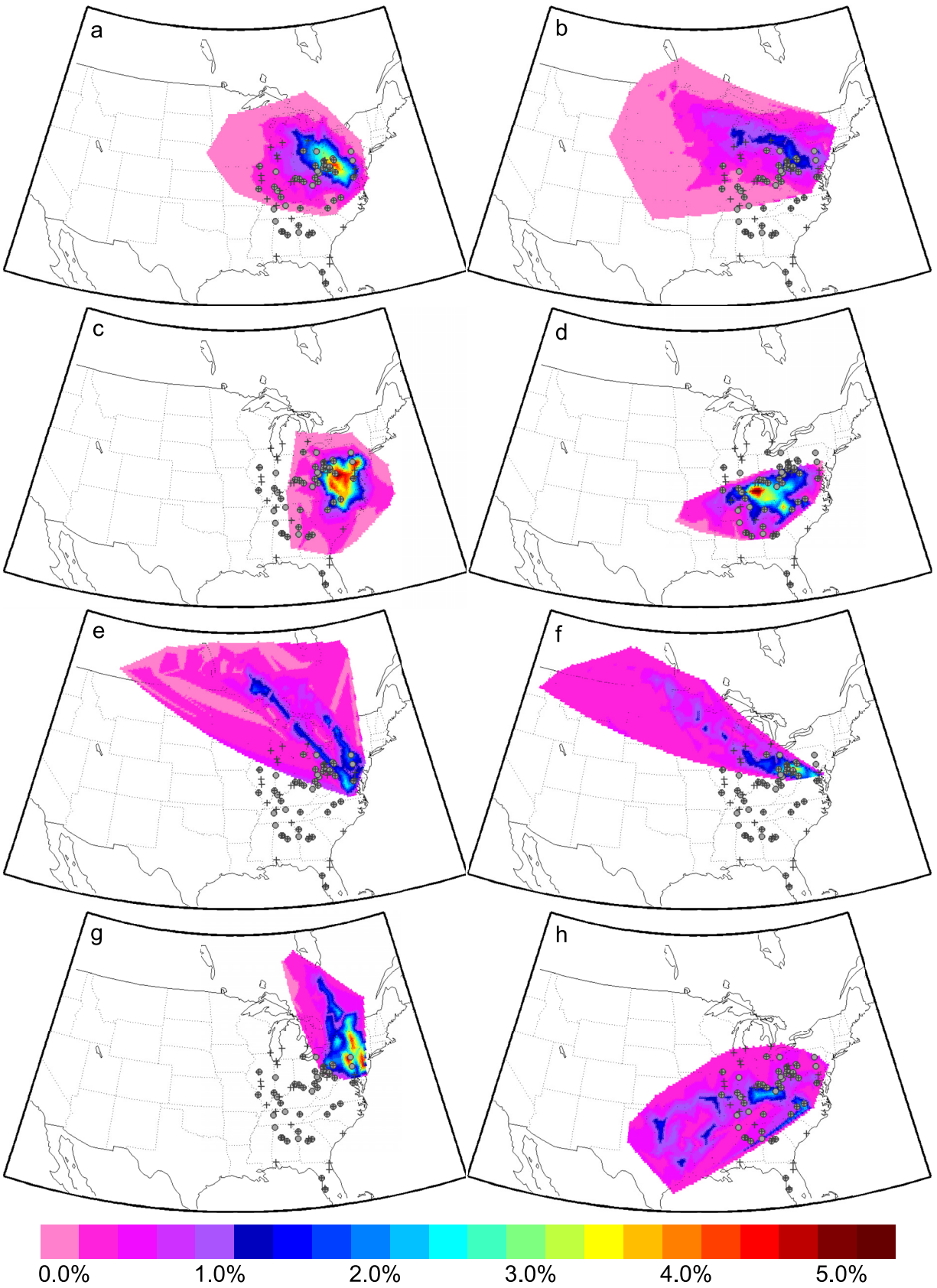


Figure 4

850 mb geopotential heights from all days that made up each cluster (Figure 5). The meteorology during these episodes is generally characterized by the extension of a well-developed Bermuda high westward into the eastern United States with a low-pressure system positioned over the eastern Canadian coastline. The meteorology of each cluster, then, may be described as a variation of this general pattern, modulated by the juxtaposition of these high- and low-pressure areas. The east/west variability of these pressure systems typically determines the wind direction. The north/south variability changes the pressure gradient, which ultimately determines the wind speed. The variations are often small; however, small variations are important because the resulting differences in wind speed and direction lead to statistically different pollution loadings over the receptor sites.

[28] Determining the statistical difference among the constituents associated with each cluster necessitated first subdividing the clusters into morning and afternoon profiles according to the aforementioned criteria. For all trace gas profiles except morning  $O_3$ , the boundary layer (defined as the layer between 100 m and 2 km) column content (in  $\text{matm-cm}$ ) was calculated. For morning  $O_3$ , the residual layer (defined as the layer between 500 m and 2 km) column content (also in  $\text{matm-cm}$ ) was quantified to capture the impacts of regionally transported pollution on the receptor locations. For the aerosol profiles, the extinction weighted  $\omega_{0.550}$  column average, aerosol optical depth at 550 nm between the surface and 3 km (AOD), and scattering weighted  $\alpha$  were calculated. The cluster median values were then determined. The cluster median ranks are given in Table 2 and the cluster median values for the extinction weighted  $\omega_{0.550}$  and AOD are given in Table 3.

[29] Using the individual profile values, the difference between the cluster medians was calculated using a multiple comparison procedure with statistical values generated from the Kruskal-Wallis test. This test is similar to the standard one-way analysis of variance, but is a nonparametric version. The requisite assumption of the one-way analysis of variance that the data are normally distributed is relaxed in the Kruskal-Wallis test such that the data must only be continuously distributed. The test ranks the values and performs an analysis of variance on the ranks rather than the values themselves. For this study, the cutoff for the probability value (p-value) was set to 0.05. When the p-value was less than this limit, the null hypothesis was rejected and the cluster medians were declared statistically different with greater than 95% confidence. The results are summarized in Table 4.

### 3.2. Pollution Profiles

[30] Figures 6 and 7 show the morning and afternoon median vertical profiles, respectively, for each constituent. Cluster 1, associated with large amounts of  $O_3$ , a large  $SO_2/CO$  ratio, large, highly scattering particles, and a large AOD (Figures 6a–6e and 7a–7e and Tables 2 and 3), shows

moderate northwesterly flow. These values are indicative of aged point source pollution. The greatest trajectory density in this cluster lies over the northern Ohio River Valley where there are several large  $NO_x$  and  $SO_2$  sources (Figure 4a). Fresh  $NO_x$  and  $SO_2$  emissions from these sources have had ample opportunity under a moderate flow regime to produce  $O_3$  and secondary aerosols en route to the mid-Atlantic.

[31] Cluster 2 shows similar wind direction to cluster 1, but with higher wind speeds (Figure 3b). The greatest trajectory density also lies mainly over the northern Ohio River Valley and extends into the Great Lakes region (Figure 4b). The particles are also large and highly scattering, but the AOD is lower (Figures 6d, 6e, 7d, and 7e and Tables 2 and 3). The CO is even less than in cluster 1, the  $SO_2/CO$  ratio is large, and the  $O_3$  values, particularly in the afternoon, are small (Figures 6a–6c and 7a–7c and Table 2). These values are all consistent with northwesterly flow similar to cluster 1 that brings northern Ohio River Valley point source pollution, but with higher wind speeds, so that there is less time for local, photochemical  $O_3$  production or mixing with urban, mobile source pollution. Figure 4b shows that, in fact, the greatest trajectory density intersects many large  $NO_x$  and  $SO_2$  sources.

[32] Cluster 3 is typified by stagnant conditions with light, southerly flow (Figure 3c). The greatest air parcel density is found over the central mid-Atlantic region. Ozone values, particularly in the afternoon, are large, as are CO values, whereas  $SO_2$  values, especially in the morning, are small (Figures 6a–6c and 7a–7c and Table 2). Hence the  $SO_2/CO$  ratio is small (Table 2). The particle property values are moderate (Figures 6d, 6e, 7d, and 7e and Tables 2 and 3). These values, together with the stagnant conditions associated with cluster 3, indicate local, urban, mobile source-dominated pollution. Figure 4c shows that there are few large  $NO_x$  and  $SO_2$  sources in the area of greatest trajectory density. Presumably, because there is less hygroscopic  $SO_4^{2-}$  available for particle growth, the particles are smaller and less scattering than in the first two clusters.

[33] The transport pattern identified by cluster 4 is characterized by moderate southwesterly flow and the greatest trajectory density lies over the southern Ohio River Valley (Figures 3d and 4d). For the most part, this cluster is associated with little pollution loading and the  $SO_2/CO$  ratio is small (Figures 6a–6e and 7a–7e and Tables 2 and 3), suggesting that there are fewer point sources located farther south along the Ohio River. Figure 4d shows no large  $NO_x$  or  $SO_2$  sources in the area of greatest trajectory density, although many do encircle this area. Also, the afternoon  $O_3$  values are particularly small, and not much larger than the morning values (Figures 6a and 7a and Table 2), indicating there was little photochemical production during transport of the air parcels. Figure 5d shows the greatest 850 mb geopotential heights farther to the south than the other clusters, so mid-Atlantic regional temper-

**Figure 4.** Trajectory density maps for (a) cluster 1, (b) cluster 2, (c) cluster 3, (d) cluster 4, (e) cluster 5, (f) cluster 6, (g) cluster 7, and (h) cluster 8. The plots were generated using a linear interpolation method between the trajectory end points. They indicate the relative density (%) of air parcels over the total area described by the spaghetti plots. Also pictured are the locations of the top 0.3% emitters annually of  $NO_x$  (grey circles) and  $SO_2$  (crosses) in the eastern United States.

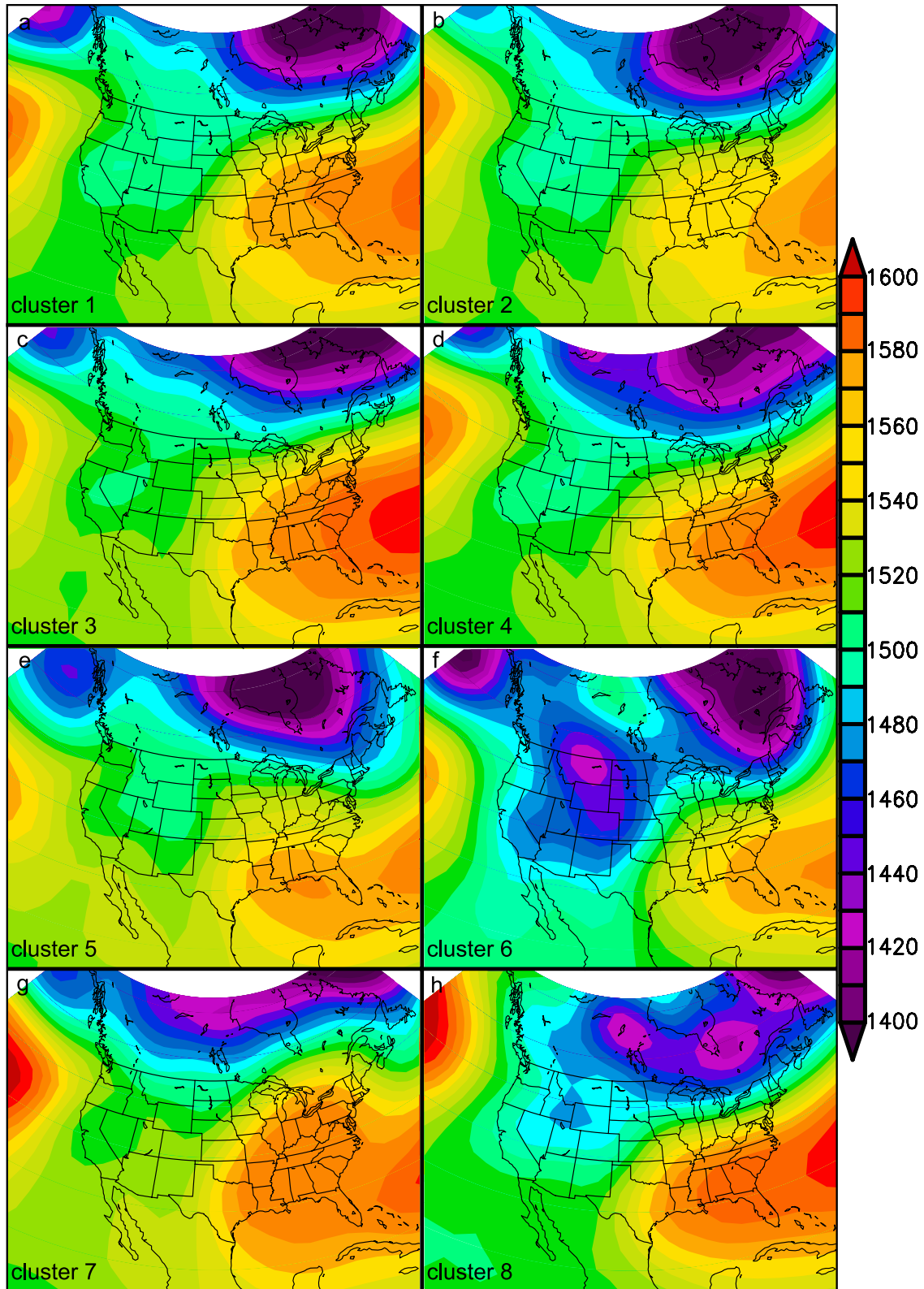


**Figure 5.** Composite mean 850 mb geopotential heights (m) for (a) cluster 1, (b) cluster 2, (c) cluster 3, (d) cluster 4, (e) cluster 5, (f) cluster 6, (g) cluster 7, and (h) cluster 8 generated using NCEP reanalysis data from the NOAA-CIRES Climate Diagnostics Center.

**Table 2.** Cluster Median Profile Ranks, % O<sub>3</sub> Transported, and Cluster Median Column Content SO<sub>2</sub>/CO Ratios for the Morning (First Number) and Afternoon (Second Number)<sup>a</sup>

Clusters	Median O <sub>3</sub> Rank	% O <sub>3</sub> Transported	Median CO Rank	Median SO <sub>2</sub> Rank	SO <sub>2</sub> /CO	Median $\omega_{0.550}$ Rank	Median AOD Rank	Median $\alpha$ Rank
1 (107, 26.3)	1, 2	70 ± 17 <sup>b</sup>	4, 7	4, 2	0.014, 0.017	2, 1	1, 1	6, 7
2 (77, 19.0)	4, 5	69 ± 21	8, 8	5, 4	0.015, 0.016	1, 2	2, 2	7, 6
3 (108, 26.6)	3, 1	58 ± 25	3, 3	7, 3	0.009, 0.011	3, 4	3, 4	4, 4
4 (39, 9.6)	6, 8	82 ± 25	7, 2	8, 6	0.010, 0.006	4, 3	5, 3	2, 5
5 (24, 5.9)	5, 3	62 ± 27	5, 6	3, 7	0.015, 0.008	5, 5	6, 7	1, 1
6 (15, 3.7)	2, 4	73 ± 28	2, 4	1, 1	0.026, 0.016	6, 7	4, 5	3, 3
7 (23, 5.7)	8, 7	56 ± 27	6, 5	6, 8	0.013, 0.008	7, 6	7, 6	5, 2
8 (13, 3.2)	7, 6	55 ± 12	1, 1	2, 5	0.008, 0.006	*	*	*

<sup>a</sup>Values in parentheses to the right of the cluster number are the total profiles that went into that cluster (left) and the percent of the total profiles (right). Asterisks indicate insufficient data to calculate statistical values for cluster 8.

<sup>b</sup>Error estimated by adding in quadrature 1  $\sigma$  from the residual layer and afternoon boundary layer mean values.

atures were probably not great enough to initiate considerable photochemical production.

[34] Cluster 5 shows fairly fast north-northwesterly flow over the northern Great Lakes region into the mid-Atlantic region (Figure 3e). Generally, this flow pattern seems to transport little pollution into the region. However, the O<sub>3</sub> values are large below ~1.2 km in the morning (Figure 6a) and ~1.5 km in the afternoon (Figure 7a) and only fall off to lower values aloft. The areas of greatest trajectory density do intersect large NO<sub>x</sub> and SO<sub>2</sub> sources (Figure 4e), a fact corroborated by a high SO<sub>2</sub>/CO ratio in the morning (Table 2), but the wind speeds, particularly aloft, are too great to allow for pollution to accumulate in the mid-Atlantic region. The fast wind speeds are also not conducive to particle growth, so the smallest particles are found in this cluster (Figures 6e and 7e and Table 2).

[35] The wind direction of the trajectories in cluster 6 is northwesterly as in clusters 1 and 2, with still faster wind speeds than in cluster 2 (Figure 3f). The greatest trajectory density again lies over the northern Ohio River Valley and several large NO<sub>x</sub> and SO<sub>2</sub> sources (Figure 4f). The pollution loadings of this cluster are also consistent with these sources, but because of the higher wind speeds, the pollution appears to be relatively fresher. The O<sub>3</sub> values are moderately large, with smaller values in the afternoon, the CO values are moderate, and the SO<sub>2</sub> values are very large, so that the SO<sub>2</sub>/CO ratio is also very large (Figures 6a–6c and 7a–7c and Table 2). The SO<sub>2</sub> apparently did not have much opportunity for oxidation before entering the mid-Atlantic region. The particles were smaller and less scattering and the AOD was smaller than in clusters 1 and 2 (Figures 6d–6e and 7d–7e and Tables 2 and 3).

**Table 3.** Cluster Median Profile Values for the Morning and Afternoon Aerosol Extinction Weighted  $\omega_{0.550}$  and AOD

Clusters <sup>a</sup>	Morning $\omega_{0.550}$	Afternoon $\omega_{0.550}$	Morning AOD	Afternoon AOD
1	0.91 ± 0.05 <sup>b</sup>	0.95 ± 0.04	0.37 ± 0.19	0.35 ± 0.30
2	0.91 ± 0.06	0.94 ± 0.05	0.31 ± 0.23	0.31 ± 0.25
3	0.90 ± 0.06	0.93 ± 0.04	0.30 ± 0.28	0.26 ± 0.12
4	0.88 ± 0.06	0.94 ± 0.03	0.22 ± 0.06	0.29 ± 0.07
5	0.87 ± 0.08	0.91 ± 0.05	0.17 ± 0.10	0.15 ± 0.10
6	0.82 ± 0.09	0.85 <sup>c</sup>	0.25 ± 0.08	0.25 <sup>c</sup>
7	0.81 ± 0.17	0.85 ± 0.12	0.15 ± 0.12	0.20 ± 0.12

<sup>a</sup>There were not enough data to calculate statistical values for cluster 8.

<sup>b</sup>The error represents 1  $\sigma$  of the cluster mean value.

<sup>c</sup>No error is given because there was only one profile that went into the cluster 6 afternoon  $\omega_{0.550}$  and AOD values.

[36] Overall, cluster 7 is associated with the least pollution of any of the clusters (Figures 6a–6e and 7a–7e and Tables 2 and 3). The flow is out of the north, bringing relatively cool, dry, continental air to the mid-Atlantic region (Figure 5g). There are no major urban centers, nor are there many NO<sub>x</sub> or SO<sub>2</sub> sources in the area of greatest trajectory density (Figure 4g).

[37] Cluster 8 comprises very few trajectories. The flow is fast and from the southwest, originating near Texas (Figure 3h). There were not enough particle data to generate any statistical values. The O<sub>3</sub> values are small, the SO<sub>2</sub> values are moderate, and the CO is very large (Figures 6a–6c and 7a–7c and Table 2). The areas of greatest trajectory density do not intersect many large NO<sub>x</sub> or SO<sub>2</sub> sources (Figure 4h). Given the large CO values, small SO<sub>2</sub>/CO ratio, and trajectory densities, the air parcels may have entrained local, mobile emissions or upwind, industrial or biogenic VOC emissions that were oxidized during transport. Figure 8 summarizes the transport from the areas of greatest trajectory density into the mid-Atlantic region as a percent of the total number of profiles examined in this study.

### 3.3. O<sub>3</sub> Transport

[38] Thus far, the first of the two original questions posed has been addressed. Namely, a statistical link between characteristic regional transport patterns into the mid-Atlan-

**Table 4.** Statistical Difference Among Cluster Morning and Afternoon Profile Median Values<sup>a</sup>

	Clusters							
	1	2	3	4	5	6	7	8
Morning O <sub>3</sub>	>7, 8	*	>8	*	*	>8	<1	<1, 3, 6
Afternoon O <sub>3</sub>	>4	<3	>2, 4, 7	<1, 3	*	*	<3	*
Morning CO	*	<8	*	<8	*	*	*	>2, 4
Afternoon CO	*	*	*	*	*	*	*	*
Morning SO <sub>2</sub>	*	*	<6	<6	*	>3, 4	*	*
Afternoon SO <sub>2</sub>	*	*	*	*	*	*	*	*
Morning $\omega_{0.550}$	*	*	*	*	*	*	*	*
Afternoon $\omega_{0.550}$	*	*	*	*	*	*	*	*
Morning AOD	>4, 5	*	*	<1	<1	*	*	*
Afternoon AOD	>5	>5	*	*	<1, 2	*	*	*
Morning $\alpha$	<5	<5	*	*	>1, 2, 7	*	<5	*
Afternoon $\alpha$	<5, 7	*	*	*	>1	*	>1	*

<sup>a</sup>The > (<) signifies that the median value for the cluster is statistically greater (less) than, with 95% confidence, the median values of the cluster numbers listed after the symbol. Asterisks indicate no statistical difference between that particular cluster median value and other cluster median values.

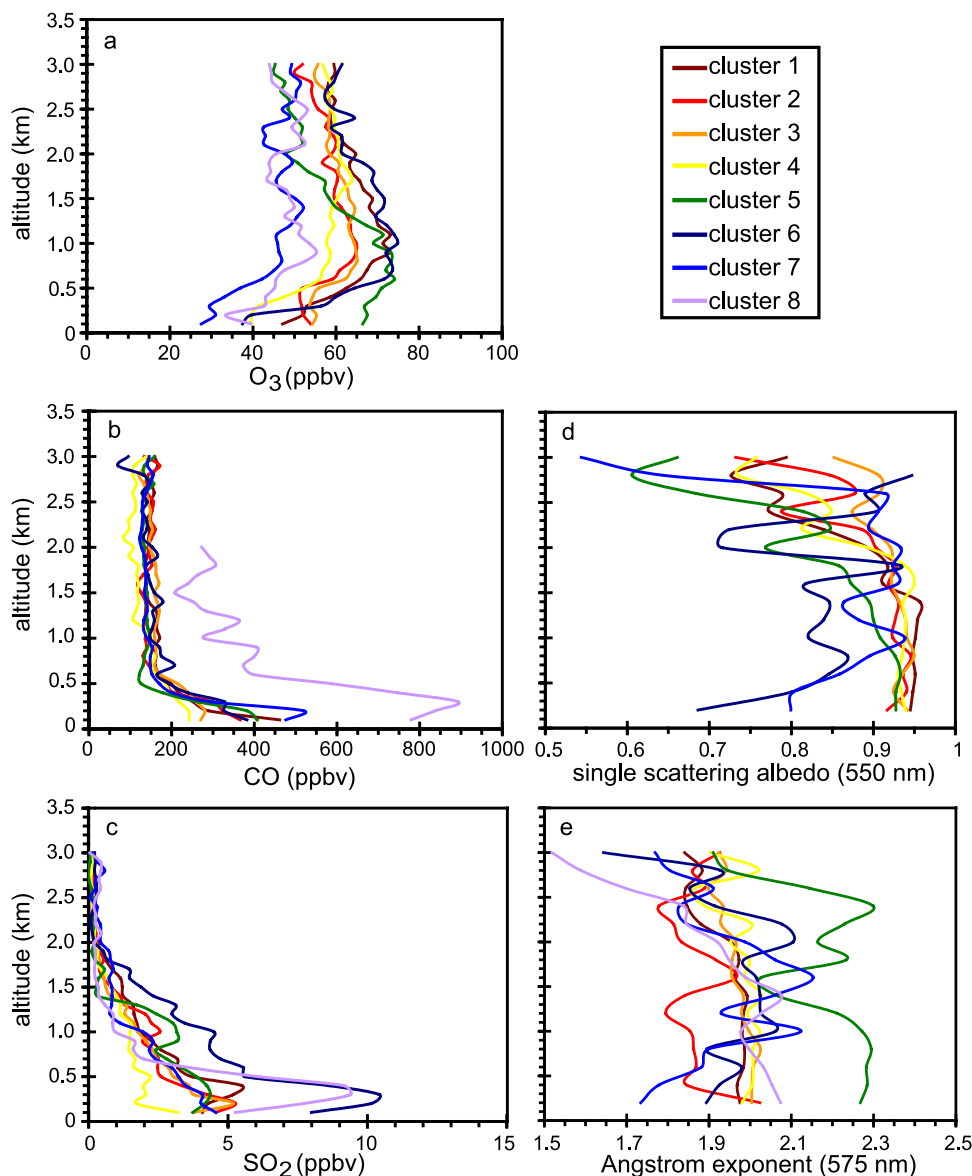


**Figure 6.** Median morning (before 1200 LST) profiles for clusters 1 (brown), 2 (red), 3 (orange), 4 (yellow), 5 (green), 6 (dark blue), 7 (blue), and 8 (violet) of (a)  $O_3$ , (b) CO, (c)  $SO_2$ , (d) single scattering albedo (550 nm), and (e) Ångström exponent (575 nm).

tic during summertime haze and  $O_3$  episodes and specific pollution loadings has been established. In this section, the contribution of regionally transported  $O_3$  to afternoon boundary layer  $O_3$  over the mid-Atlantic will be quantified.

[39] The percent of the afternoon  $O_3$  boundary layer column content for each cluster that can be accounted for by regional transport was estimated with the following equation:

$$\% O_3 \text{ transported} = \left( \frac{RL}{MBL} \right) \times \left( \frac{MBL}{ABL} \right) \times 100, \quad (2)$$

where  $RL$  is the residual layer (defined as the layer between 500 m and 2 km in the morning profiles) column content,  $MBL$  is the morning boundary layer (defined as the layer between 100 m and 2 km in the morning profiles) column

content, and  $ABL$  is the afternoon boundary layer (defined as the layer between 100 m and 2 km in the afternoon profiles) column content. The equation simplifies to the ratio of  $RL/ABL$  after the  $MBL$ s cancel out. Assuming the  $RL$   $O_3$  was transported to the morning spiral location from an upwind regional source and subsequently transported to the afternoon spiral location where it mixed with the locally produced  $O_3$  to give the  $ABL$   $O_3$  column content, the equation should provide the relative contribution of regionally transported  $O_3$  to the afternoon boundary layer column content. The accuracy of this method depends upon the Lagrangian nature of the morning and afternoon profiles from each cluster. Because flight plans were designed in a Lagrangian manner, where morning flights were upwind of afternoon flights, the estimate should be accurate. The results are shown in Table 2 and Figure 9. The amount of afternoon  $O_3$  that can be accounted for by regional transport

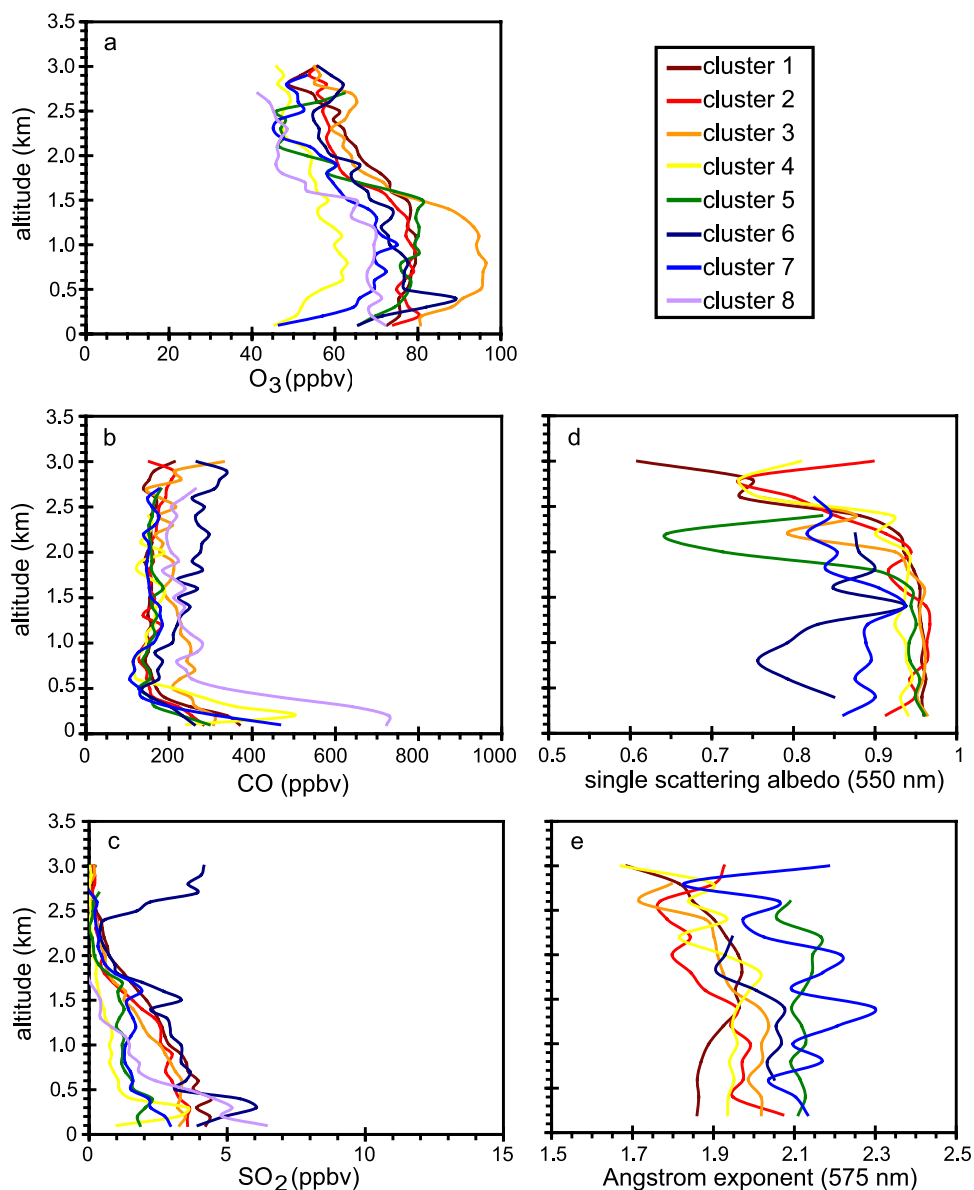


**Figure 7.** Median afternoon (after 1200 LST) profiles for clusters 1 (brown), 2 (red), 3 (orange), 4 (yellow), 5 (green), 6 (dark blue), 7 (blue), and 8 (violet) of (a) O<sub>3</sub>, (b) CO, (c) SO<sub>2</sub>, (d) single scattering albedo (550 nm), and (e) Ångström exponent (575 nm).

ranges from a low of 55% to a high of 82%. One of the smallest contributions from transport (58%) corresponds to cluster 3. This cluster shows the most stagnant conditions so that transport would not be expected to contribute as much to the afternoon totals. The largest contributions from regional transport are seen in clusters 1(70%), 2(69%), 4(82%) and 6(73%). The corresponding trajectory density plots (Figures 4a, 4b, 4d, and 4f) show that their greatest air parcel densities are over the Ohio River Valley. Those of cluster 4 lie over the southern Ohio River Valley (Figure 4d) whereas those of the other three clusters all lie over the northern portion of the Ohio River (Figures 4a, 4b, and 4f). The pollution loadings associated with cluster 4 are relatively small, but those in clusters 1, 2, and 6, particularly with respect to O<sub>3</sub>, SO<sub>2</sub>, and particle pollution, are large. In general, the greatest regional O<sub>3</sub> transport was from the

Ohio River Valley, while some of the least transport occurred during clean, northerly flow (cluster 7) and when stagnant conditions persisted and photochemical production was highest (cluster 3).

#### 4. Conclusions

[40] Several years of episodic, summertime aircraft vertical profile trace gas and aerosol data collected as part of RAMMPP were analyzed in this study. Initially, the data were divided into morning and afternoon profiles to identify diurnal patterns. Little diurnal variation was observed in the CO, SO<sub>2</sub>, or Ångström exponent, although the Ångström exponent decreased with altitude. O<sub>3</sub> values were greater in the afternoon than the morning, while O<sub>3</sub> in the lower free troposphere, amenable to long-range transport, was consis-

tently  $\sim 55$  ppbv. The single scattering albedo was larger in the afternoon than the morning, likely the result of  $\text{SO}_2$  oxidation to  $\text{SO}_4^{2-}$ . A decrease in the single scattering albedo above 2 km was due to invariant absorption values with altitude combined with scattering values that declined with altitude.

[41] Characteristic transport patterns and source regions during summertime haze and  $\text{O}_3$  episodes were analyzed with an agglomerative hierarchical cluster analysis of back trajectory data. Eight clusters were identified, which were then divided into morning and afternoon profiles. The median profile values were calculated and statistical differences were determined using a nonparametric procedure. When the greatest trajectory density lay over the northern Ohio River Valley and large  $\text{NO}_x$  and  $\text{SO}_2$  sources, the result was large  $\text{O}_3$  values, a large  $\text{SO}_2/\text{CO}$  ratio, large, scattering particles, and high AOD over the mid-Atlantic United States. In contrast, relatively clean conditions over the mid-Atlantic occurred when the greatest trajectory density lay over the southern Ohio River Valley and nearly missed many large  $\text{NO}_x$  and  $\text{SO}_2$  sources. The greatest afternoon  $\text{O}_3$  occurred during periods of stagnation that were most conducive to photochemical production. The least pollution occurred when flow from the north-northwest was too fast for pollution to accumulate and when flow was from the north, where there are few urban or industrial sources.

[42] Ozone transport over several hundred kilometers into the mid-Atlantic United States was estimated by calculating the ratio of the residual layer  $\text{O}_3$  in the upwind morning profiles to the downwind afternoon boundary layer values. The greatest  $\text{O}_3$  transport (69–82%) occurred when the maximum trajectory density lay over the southern and northern Ohio River Valley ( $\sim 59\%$  of the total profiles). The least  $\text{O}_3$  transport (55–58%) was associated with fast southwesterly flow ( $\sim 3\%$  of the total profiles), clean

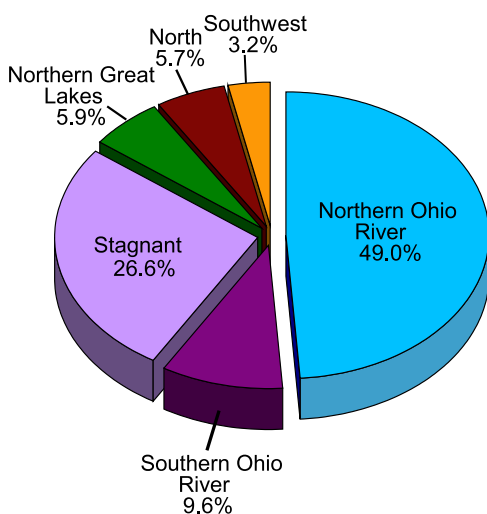


**Figure 8.** Pie chart showing the transport from the particular areas, as defined by the trajectory densities in each cluster, into the mid-Atlantic region as a percent of the total number of profiles examined in the study. The Northern Ohio River slice comprises clusters 1, 2, and 6.

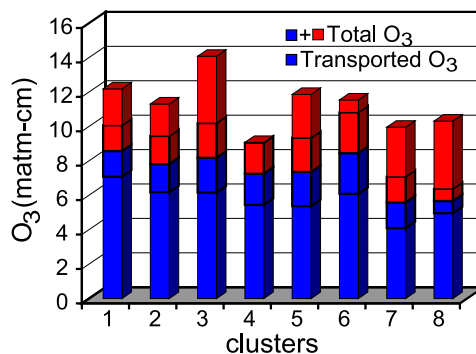


**Figure 9.** Bar chart showing the total afternoon boundary layer column  $\text{O}_3$  content (red + blue) and the contribution from regional transport (blue) for each cluster. The error associated with the transported  $\text{O}_3$  was estimated by adding in quadrature  $1 \sigma$  from the residual layer and afternoon boundary layer mean values and is indicated by the dark lines above and below the transported  $\text{O}_3$  column content.

northerly flow ( $\sim 6\%$  of the total profiles), and stagnant, polluted conditions ( $\sim 27\%$  of the total profiles).

[43] In summary, this investigation demonstrated the ability to identify statistically significant differences among pollution profiles that resulted from seemingly minor variations of the typical summertime, polluted meteorological regime. When trajectory density plots were overlaid on maps with the largest annual  $\text{NO}_x$  and  $\text{SO}_2$  emitters, specific source regions were identified. The results indicate that the areas of maximum trajectory density together with wind speed are effective predictors of regional pollutant loadings. Additionally, because of the Lagrangian nature of the data set, the regionally transported contribution to the total afternoon boundary layer column  $\text{O}_3$  content in each cluster could be quantified.

[44] **Acknowledgments.** Support for this work was provided by the Pennsylvania State University, Department of Meteorology and the Maryland Department of Environment through the University of Maryland. Funding for the experimental work was provided by NARSTO-Northeast through EPRI, USEPA through NARSTO/NE-OPS, the Virginia Department of Environmental Quality, the North Carolina Division of Air Quality, NESCAUM through MANE-VU, and the DOE National Energy Technology Laboratory. Composite meteorological images were provided by the NOAA-CIRES Climate Diagnostics Center, Boulder, Colorado, from their Web site at <http://www.cdc.noaa.gov/>.

## References

- Anderson, T. L., and J. A. Ogren (1998), Determining aerosol radiative properties using the TSI 3563 Integrating Nephelometer, *Aerosol Sci. Technol.*, *29*, 57–69.
- Anderson, T. L., et al. (1996), Performance characteristics of a high-sensitivity, three-wavelength, total scatter/backscatter nephelometer, *J. Atmos. Oceanic Technol.*, *13*, 967–986.
- Anderson, T. L., D. S. Covert, J. D. Wheeler, J. M. Harris, K. D. Perry, B. E. Trost, and D. J. Jaffe (1999), Aerosol backscatter fraction and single scattering albedo: Measured values and uncertainties at a coastal station in the Pacific NW, *J. Geophys. Res.*, *104*, 26,793–26,807.
- Ashbaugh, L. L. (1983), A statistical trajectory technique for determining air pollution source regions, *J. Air Pollut. Control Assoc.*, *33*, 1096–1098.
- Berto, A., A. Buzzi, and D. Zardi (2004), Back-tracking water vapour contributing to a precipitation event over Trentino: A case study, *Meteorol. Z.*, *13*(3), 189–200.
- Bond, T. C., T. L. Anderson, and D. Campbell (1999), Calibration and intercomparison of filter-based measurements of visible light absorption by aerosols, *Aerosol Sci. Technol.*, *30*, 582–600.

- Brankov, E., S. T. Rao, and P. S. Porter (1998), A trajectory-clustering-correlation methodology for examining the long-range transport of air pollutants, *Atmos. Environ.*, *32*(9), 1525–1534.
- Cape, J. N., J. Methven, and L. E. Hudson (2000), The use of trajectory cluster analysis to interpret trace gas measurements at Mace Head, Ireland, *Atmos. Environ.*, *34*, 3561–3663.
- Dickerson, R. R., and A. C. Delany (1988), Modification of a commercial gas filter correlation CO detector for increased sensitivity, *J. Atmos. Oceanic Technol.*, *5*(3), 424–431.
- Dickerson, R. R., B. G. Doddridge, P. K. Kelley, and K. P. Rhoads (1995), Large-scale pollution of the atmosphere over the North Atlantic Ocean: Evidence from Bermuda, *J. Geophys. Res.*, *100*(5), 8945–8952.
- Doddridge, B. G., R. M. Morales, K. P. Rhoads, J. T. Merrill, P. C. Novelli, R. R. Dickerson, V. S. Connors, and H. G. Reichle Jr. (1998), Ground-based and airborne observations of carbon monoxide during NASA/ MAPS missions SRL-1 and SRL-2, *J. Geophys. Res.*, *103*, 19,305–19,316.
- Dorling, S. R., and T. D. Davies (1995), Extending cluster analysis—Synoptic meteorology links to characterise chemical climates at six north-west European monitoring stations, *Atmos. Environ.*, *29*(2), 145–167.
- Dorling, S. R., T. D. Davies, and C. E. Pierce (1992a), Cluster analysis: A technique for estimating the synoptic meteorological controls on air and precipitation chemistry—Method and applications, *Atmos. Environ., Part A*, *26*(14), 2575–2582.
- Dorling, S. R., T. D. Davies, and C. E. Pierce (1992b), Cluster analysis: A technique for estimating the synoptic meteorological controls on air and precipitation chemistry—Results from Eskdalemuir, S. Scotland, *Atmos. Environ., Part A*, *26*(14), 2583–2602.
- Draxler, R. R., and G. D. Rolph (2003), HYSPLIT (Hybrid Single-Particle Lagrangian Integrated Trajectory) Model access via NOAA ARL READY website, NOAA Air Resour. Lab., Silver Spring, Md. (Available at <http://www.arl.noaa.gov/ready/hysplit4.html>)
- Eneroth, K., E. Kjellstrom, and K. Holmen (2003), A trajectory climatology for Svalbard; investigating how atmospheric flow patterns influence observed tracer concentrations, *Phys. Chem. Earth*, *28*, 1191–1203.
- Harris, J. M., and S. J. Oltmans (1997), Variations in tropospheric ozone related to transport at American Samoa, *J. Geophys. Res.*, *102*(D7), 8781–8791.
- Jorba, O., C. Perez, F. Rocadenbosch, and J. M. Baldasano (2004), Cluster analysis of 4-day back trajectories arriving in the Barcelona area, Spain, from 1997 to 2002, *J. Appl. Meteorol.*, *43*(6), 887–901.
- Kalkstein, L. S., G. Tan, and J. A. Skindlov (1987), An evaluation of three clustering procedures for use in synoptic climatological classification, *J. Appl. Meteorol.*, *26*, 717–730.
- Kalnay, E., et al. (1996), The NCEP/NCAR reanalysis 40-year project, *Bull. Am. Meteorol. Soc.*, *77*, 437–471.
- Kleinman, L. I., and P. H. Daum (1991), Oxidant limitation to the formation of H<sub>2</sub>SO<sub>4</sub> near a SO<sub>2</sub> source region, *Atmos. Environ.*, *25*(9), 2023–2028.
- Lee, G., J. T. Merrill, and B. J. Huebert (1994), Variation of free tropospheric total nitrate at Mauna Loa Observatory, *Hawaii, J. Geophys. Res.*, *99*(D6), 12,821–12,831.
- Logan, J. A. (1985), Tropospheric ozone: Seasonal behavior trends and anthropogenic influence, *J. Geophys. Res.*, *90*, 10,463–10,482.
- Luke, W. T. (1997), Evaluation of a commercial pulsed fluorescence detector for the measurement of low-level SO<sub>2</sub> concentrations during the Gas-Phase Sulfur Intercomparison Experiment, *J. Geophys. Res.*, *102*(D13), 16,255–16,265.
- Marufu, L. T., B. F. Taubman, B. Bloomer, C. A. Piety, B. G. Doddridge, and R. R. Dickerson (2004), The 2003 North American electrical blackout: An accidental experiment in atmospheric chemistry, *Geophys. Res. Lett.*, *31*, L13106, doi:10.1029/2004GL019771.
- Moody, J. L., and J. N. Galloway (1988), Quantifying the relationship between atmospheric transport and the chemical composition of precipitation on Bermuda, *Tellus, Ser. B*, *40*, 463–479.
- Moody, J. L., S. J. Oltmans, H. Levy II, and J. T. Merrill (1995), Transport climatology of tropospheric ozone: Bermuda, 1988–1991, *J. Geophys. Res.*, *100*(D4), 7179–7194.
- Moody, J. L., J. W. Munger, A. H. Goldstein, D. J. Jacob, and S. C. Wofsy (1998), Harvard Forest regional-scale air mass composition by Patterns in Atmospheric Transport History (PATH), *J. Geophys. Res.*, *103*(D11), 13,181–13,194.
- Moy, L. A., R. R. Dickerson, and W. F. Ryan (1994), Relationship between back trajectories and tropospheric trace gas concentrations in rural Virginia, *Atmos. Environ.*, *28*(17), 2789–2800.
- Novakov, T., D. A. Hegg, and P. V. Hobbs (1997), Airborne measurements of carbonaceous aerosols on the East Coast of the United States, *J. Geophys. Res.*, *102*, 30,023–30,030.
- Russell, A., G. R. McGregor, and G. J. Marshall (2004), An examination of the precipitation delivery mechanisms for Doleman Island, eastern Antarctic Peninsula, *Tellus, Ser. A*, *56*, 501–513.
- Ryan, W. F., B. G. Doddridge, R. R. Dickerson, R. M. Morales, K. A. Hallock, P. T. Roberts, D. L. Blumenthal, J. A. Anderson, and K. L. Civerolo (1998), Pollutant transport during a regional O<sub>3</sub> episode in the mid-Atlantic states, *J. Air Waste Manage. Assoc.*, *48*, 786–797.
- Stohl, A. (1998), Computation, accuracy and applications of trajectories—A review and bibliography, *Atmos. Environ.*, *32*(6), 947–966.
- Stohl, A., and P. Seibert (1998), Accuracy of trajectories as determined from the conservation of meteorological tracers, *Q. J. R. Meteorol. Soc.*, *124*(549), 1465–1484.
- Stohl, A., G. Wotawa, P. Seibert, and H. Kromp-Kolb (1995), Interpolation errors in wind fields as a function of spatial and temporal resolution and their impact on different types of kinematic trajectories, *J. Appl. Meteorol.*, *34*, 2149–2165.
- Stunder, B. J. B. (1996), An assessment of the quality of forecast trajectories, *J. Appl. Meteorol.*, *35*, 1319–1331.
- Taubman, B. F., L. T. Marufu, C. A. Piety, B. G. Doddridge, J. W. Stehr, and R. R. Dickerson (2004a), Airborne characterization of the chemical, optical, and meteorological properties, and origins of a combined ozone/haze episode over the eastern U.S., *J. Atmos. Sci.*, *61*(14), 1781–1793.
- Taubman, B. F., L. T. Marufu, B. L. Vant-Hull, C. A. Piety, B. G. Doddridge, R. R. Dickerson, and Z. Li (2004b), Smoke over haze: Aircraft observations of chemical and optical properties and the effects on heating rates and stability, *J. Geophys. Res.*, *109*, D02206, doi:10.1029/2003JD003898.

R. R. Dickerson, B. G. Doddridge, L. T. Marufu, C. A. Piety, and J. W. Stehr, Department of Meteorology, University of Maryland, College Park, MD 20742, USA.

J. C. Hains, Department of Chemistry and Biochemistry, University of Maryland, College Park, MD 20742, USA.

B. F. Taubman and A. M. Thompson, Department of Meteorology, Pennsylvania State University, University Park, PA 16802, USA. (btaubman@meteo.psu.edu)